Nanoscale

PAPER

Cite this: *Nanoscale*, 2016, **8**, 19605

Novel magnetic relaxation nanosensors: an unparalleled "spin" on influenza diagnosis†

Tyler Shelby,‡ Tuhina Banerjee,‡ Jyothi Kallu, Shoukath Sulthana, Irene Zegar and Santimukul Santra*

Received 26th July 2016,
Accepted 10th October 2016

DOI: 10.1039/c6nr05889b

www.rsc.org/nanoscale

Rapid detection and diagnosis of pathogenic strains of influenza is necessary for expedited treatment and quicker resolutions to the ever-rising flu pandemics. Considering this, we propose the development of novel magnetic relaxation nanosensors (MRnS) for the rapid detection of influenza through targeted binding with hemagglutinin. 2,6- and 2,3-sialic acid ligands and entry blocker peptides are conjugated to iron oxide nanoparticles to create functional MRnS. Positive detection of various hemagglutinin variants (H1 and H5) is possible with protein concentrations as little as 1.0 nM. Most importantly, detection using functional MRnS is achieved within minutes and differentiates between influenza subtypes. This specificity allows mixtures of MRnS to screen for multiple pathogens at once, discarding the need to conduct multiple individual tests. Current methods used to diagnose influenza, such as RT-PCR and viral culturing, while largely effective, are complex, time-consuming and costly. As well, they are not as sensitive or specific, and have been known to produce false-positive results. In contrast to these methods, targeted MRnS are robust, point-of-care diagnostic tools featuring simple, rapid and low-cost procedures. These qualities, as well as high sensitivity and specificity, and low turnaround times, make a strong case for the diagnostic application of MRnS in clinical settings.

1. Introduction

Despite the household familiarity of its name, influenza remains a great risk to the modern world. Due to its innate ability to rapidly mutate, it is only ever a matter of time until a new pathogenic strain emerges.[1] Also due to its ability to mutate, influenza has developed resistances to a number of anti-viral treatments, which makes it difficult to both predict the next pathogenic strain and curb the resulting pandemics. Therefore, rapid detection of influenza and the ability to differentiate between viral subtypes is crucial. Viral diagnostic methods used prominently in today's clinical settings rely on the detection of antigens or antibodies present in the patient's blood, amplification of targeted genomic sequences, or isolation and culturing of the virus.[2] Some of these techniques include enzyme-linked immunosorbent assays (ELISA), viral culturing, serology, loop-mediated isothermal amplification-based assays (LAMP), and multiple variations of polymerase chain reactions (PCR).[2] While these techniques have all proven to be largely successful in detecting influenza, they are costly, complicated and time-consuming. Despite their overall success, these techniques are also known to produce false positives and negatives, hampering their reliability.[3] Furthermore, current diagnostic methods consist of technical procedures that must be conducted in a well-maintained laboratory setting, and executed by trained professionals.[4] While this is not an issue in a state-of-the-art medical facility, it does hamper their adaptability to clinical settings in developing countries, where rapid detection of infectious diseases is of the utmost importance.

In response to the need for a more efficient diagnostic method, recent research has produced promising results using nanotechnology. Nanosensors are able to overcome many of the problems faced by the aforementioned diagnostic techniques through highly specific targeting, high sensitivity, and low turnaround times. Nanotechnology-based diagnostic techniques capitalize on the unique magnetic, electronic, and luminescent properties produced by nanoparticles upon binding with targeted biomarkers. These customizable properties have the potential for more rapid and accurate detection of various pathogens.[5] In 2013, Liong *et al.* designed a method which involved detection of PCR-amplified mycobacterial genes using magnetic nanoprobes.[6] Positive identi-

Department of Chemistry and KPRC, Pittsburg State University, 1701 S. Broadway Street, Pittsburg, KS 66762, USA. E-mail: ssantra@pittstate.edu; Fax: +1-620-235-4003; Tel: +1-620-235-4861

†Electronic supplementary information (ESI) available: Synthesis of IONPs, functional MRnS, characterizations, supporting figures for ζ-potential, size measurement and Autodock 4 studies and table as described in the text. See DOI: 10.1039/c6nr05889b

‡These authors contributed equally.

fication of the genomic sequence was reported within 2.5 hours, which competes with modern PCR techniques. Nonetheless, amplification of recovered genomic material is still necessary, increasing its complexity. In a recent study conducted by Ye *et al.*, luminescence-based detection of H7 subtypes of influenza was accomplished utilizing gold nanoparticles.[7] After functionalization of their magnetic gold nanoparticles, detection of H7 subtypes was possible with turnaround times of roughly 2 hours. While this method does not require amplification of genomic samples, it still faces obstacles regarding optical quenching and longer detection times. However, these drawbacks may be addressed by the use of magnetic relaxation nanosensors (MRnS).

MRnS are on the forefront of nanotechnology-based diagnostic tools, and offer hope for the progression of nano-based diagnostics as a whole. Sensitized magnetic nanosensors have been shown to form nanoassemblies with viral proteins in solution, as detected by light scattering.[8] Further studies revealed that heat-denatured viral particles did not result in successful binding, indicating that only active viral proteins will produce positive results.[8] Furthermore, magnetic nanoparticles have not only proven successful in detection of viral proteins, but have also been shown to detect bacteria, toxins, genomic material, and even hypoxic environments caused by malignant tumors.[9] Previously,[5] we demonstrated the effective detection of *Mycobacterium avium* spp. *paratuberculosis* (MAP) using MRnS techniques. Magnetic nanosensors were customized to bind to a specific genomic sequence (IS900) particular to MAP. MAP was then detected in clinically relevant samples, including tissue and blood, and the MR-based results were compared side-by-side with PCR-based diagnosis. It was determined that detection by MRnS was more effective in terms of both time and sensitivity. The same group continued using MRnS for the detection of Anthrax Lethal Factor (ALF) in solution.[9g] In addition, MRnS were used to search for potential toxin inhibitors, as the researchers were able to assess the binding affinities of the targeting ligands towards ALF. It was suggested that successful targeting ligands possessed the potential to sequester the toxin *in vivo*. These binding assays demonstrate the effective use of functional MRnS to analyze molecular interactions.[9h] Although detection *via* MRnS has been previously recorded, it has not yet been done with the level of specificity shown in this study. Alternative conjugation of MRnS and exploitation of intrinsic binding properties of the targeted glycoproteins has allowed us to differentiate between pathogenic and non-pathogenic influenza subtypes *via* a method which may be customized for additional pathogenic agents in the future.

MRnS consist of magnetic cores surrounded by a biodegradable polymeric coating, to which various targeting ligands can be conjugated. Targeting ligands are selected based upon their binding affinity towards targeted pathogen-associated proteins. To further emphasize the potential impact of MRnS-based detection methods, it has been shown that low valency nanosensors (fewer targeting ligands conjugated to MRnS surface) outperform high valency nanosensors, which indicates that conjugation of nanosensors does not require extensive usage of expensive ligands, making this method highly cost-effective.[5] The detection capabilities of the MRnS rely on implicit magnetic interactions with water molecules in solution. As the MRnS bind to the targeted protein, these interactions are disrupted and a detectable change occurs in the sensitive magnetic resonance signal, which is based upon $T2$ proton relaxation time. Without any need for sample amplification steps, minimal binding is sufficient to produce $T2$ changes. The required laboratory equipment is portable, as well as inexpensive and the techniques are relatively simple, making this diagnostic approach ideal for detection in clinical settings, particularly in developing countries.

2. Results and discussion

2.1 Influenza detection mechanism using functional MRnS

Herein we propose a method by which MRnS techniques may be applied towards the rapid detection of influenza. Through IONP surface modification, nanoparticles have been functionalized for rapid and specific binding with hemagglutinin, the influenza-associated glycoprotein responsible for viral binding and entry. Hemagglutinin (HA) was selected as a biomarker in order to design a diagnostic method able to differentiate between influenza subtypes, including H1N1 and H5N1. HA is composed of two major subunits, HA1 and HA2. HA1 is responsible for binding to the host's cell receptors, while HA2 allows for the entry of the viral genome into the host cell's cytoplasm.[10] It has been shown that human influenza viruses (H1N1) bind preferentially to α(2,6)-linked sialic acid (2,6-SA), the cell receptor located on human lung tissue, while avian viruses (H5N1) have preferential binding interactions with avian cell receptor α(2,3)-linked sialic acid (2,3-SA).[10,11] The ability to detect influenza instantaneously, as well as to specify which strain has been detected, are qualities required for influenza diagnostic techniques to reach maximum efficiency. Capitalizing on the different binding properties of the various hemagglutinin structures allows our magnetic nanosensors to bind with heightened specificity, thus differentiating between influenza subtypes. This capability would further expedite the treatment process, allowing physicians to immediately diagnose a patient's infection and begin treatment without delaying for time-consuming lab procedures. Binding between functional MRnS and HA is analyzed using binding and competition assays,[9g,h] seen in Fig. 1.

Binding assays are conducted through preparation of solutions with a constant amount of MRnS and increasing HA concentrations. As the HA concentration increases, so too does the binding with the MRnS (Fig. 1A). This binding displaces the water molecules around the MRnS, leading to an increase in $T2$ values. Therefore, an effective binding assay will produce a positive trend correlating the concentration of the HA with subsequent MRnS binding (Fig. 1B). The $\Delta T2$ data can be normalized to a value of one, represented by a unit given the term ΔMR (magnetic relaxation). Determination of ΔMR

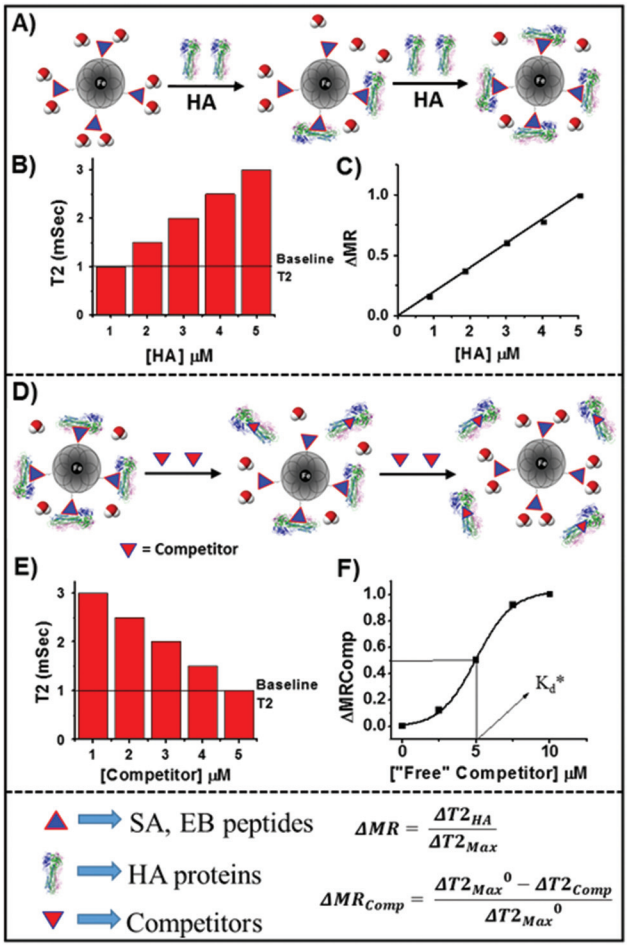

Fig. 1 Schematic representation of binding and competition assays between functional MRnS and HA. Binding assay: (A) displacement of water around the functional MRnS due to targeted binding interactions with HA, resulting in an (B) increase in *T*2 MR values as HA concentration increases. (C) These results are normalized for clearer representation as ΔMR values. Competition assay: (D) disruption of MRnS-HA binding *via* addition of "free" ligand (competitor). (E) An increase in concentration of "free" ligand causes a decrease in *T*2 MR values, which can be normalized to (F) ΔMR_{Comp} representation.

values is accomplished by dividing the Δ*T*2 value of samples with varying amounts of HA ($\Delta T2_{HA}$) by the Δ*T*2 value associated with the most concentrated HA solution ($\Delta T2_{Max}$). After normalization, the graph shows a linear increase in ΔMR values if there is successful binding. This conversion provides a clearer representation of the binding between HA and MRnS (Fig. 1C).

Competition assays are conducted by adding a "free" competitor to a solution with pre-mixed MRnS and HA (Fig. 1D). Whichever targeting ligand was used to functionalize the MRnS is also used as the competitor, and designated as "free", since it is added to the solution without being attached to IONPs. This "free" competitor then readily binds to the HA, interfering with functional MRnS binding, thus lowering the *T*2 MR signal (Fig. 1E). While verifying that the binding between functional MRnS and HA is due to the targeting ligand and not the intrinsic properties of the magnetic nanoparticle itself, this assay also allows for calculation of apparent dissociation constants (K_d^*) through the normalization of *T*2 data to ΔMR_{Comp} representation (Fig. 1F). The sigmoidal curve represents the cooperative effect of the competitor molecules as they knock proteins off the nanosensor. The ΔMR_{Comp} value is calculated by subtracting the Δ*T*2 values recorded with various concentrations of "free" competitor ($\Delta T2_{Comp}$) from the Δ*T*2 value associated with the solution having no "free" competitor ($\Delta T2^0_{Max}$), thus scaling the range of values down to zero. These values are then divided by the $\Delta T2^0_{Max}$, providing a range of ΔMR_{Comp} values between 0 and 1. The ligand concentration at which the ΔMR_{Comp} value is equal to 0.5 represents the K_d^* value. Although there are more accurate means by which true dissociation constants may be determined, the purpose of this assay is rather to produce an apparent K_d^* value which will allow for comparative binding analysis between various targeting ligands.

2.2 MRnS fabrication and influenza detection

Our IONPs were first functionalized with 2,6-SA and 2,3-SA, respectively, using carbonyldiimidazole (CDI) bioconjugation chemistry (see ESI, Scheme S1†). Briefly, carboxylated IONPs (1.0×10^{-2} M) were mixed with CDI (1.0×10^{-5} M) and incubated for 1 h at 30 °C, followed by addition of sialic acid (2,6-SA or 2,3-SA, 1.0×10^{-5} M) and continued for 3 h at room temperature. These reaction mixtures were purified using a magnetic column to obtain pure 2,6-SA and 2,3-SA functionalized MRnS with final iron concentrations of 7.5×10^{-3} M. The size and surface charge of the resulting products were characterized using a zeta-sizer and STEM, which indicated the formation of monodispersed MRnS (see ESI, Fig. S1†). In order to evaluate the potential influenza detection capability of our SA-functional MRnS, typical binding assays were performed using a constant concentration of functional MRnS (10 μL, 7.5×10^{-3} M) and increasing concentrations of hemagglutinin HA1 subunits (H1N1/HA1: 1.0×10^{-9}–1.0×10^{-7} M and H5N1/HA1: 0–6×10^{-8} M). Within 15 minutes of incubation at room temperature, a positive correlation was established between Δ*T*2 MR and hemagglutinin concentrations (Fig. 2A and C). These observations directly indicated that our functional MRnS are capable of rapidly detecting influenza-associated proteins at low concentrations. Furthermore, competition assays were conducted to verify that the binding between functional MRnS and HA was due to the presence of the targeting SA ligands. In these experiments, solutions (final volume of 500 μL) were prepared in PBS (1X, pH = 7.4) containing constant concentrations of 2,6-SA- or 2,3-SA-functional MRnS (10 μL, 7.5×10^{-3} M) and their respective HA1 subunits (5×10^{-8} M). To the corresponding solutions, increasing concentrations of "free" 2,6-SA (0–2.6×10^{-3} M) or "free" 2,3-SA (0–1.3×10^{-3} M) was added. As expected, the addition of "free" competing ligands caused a decrease in *T*2 MR values. Finally, these data were normalized to obtain ΔMR_{Comp} representation and plotted against increasing "free" ligand concentrations, as

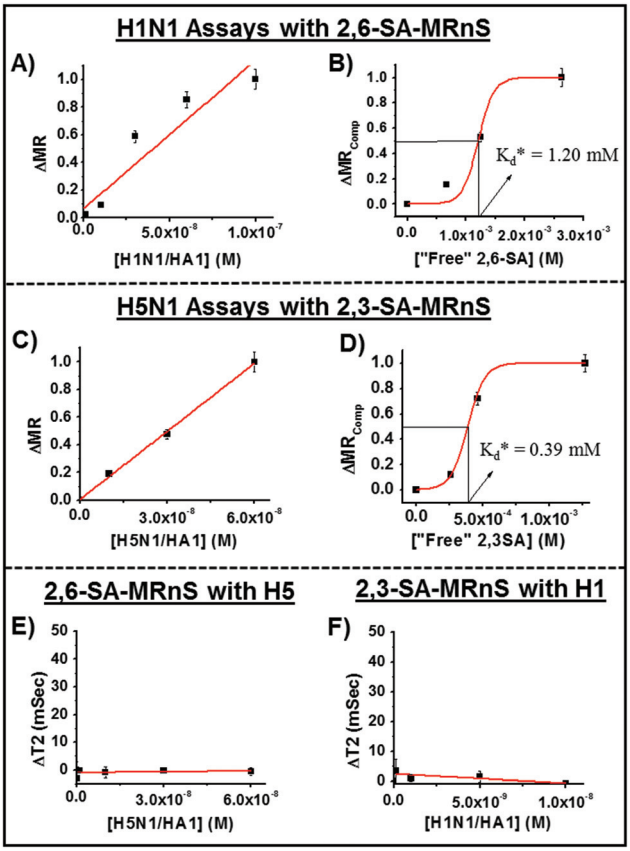

Fig. 2 (A) Binding assay for detection of H1N1 using 2,6-SA-MRnS (10 μL, 7.5×10^{-3} M), showing linear binding correlation with H1N1/HA1 concentrations (1.0×10^{-9}–1.0×10^{-7} M). (B) Corresponding competition assay with increasing concentration (0–2.6×10^{-3} M) of "free" 2,6-SA (competitor), which verified the interaction between 2,6-SA and H1N1/HA1 influenza protein (K_d^* = 1.20 mM). Similar binding assay (C) for detection of H5N1 using 2,3-SA-MRnS (10 μL, 7.5×10^{-3} M) and H5N1/HA1 subunits (0–6×10^{-8} M), and subsequent binding analysis *via* (D) competition assay using "free" 2,3-SA (0–1.3×10^{-3} M) (K_d^* = 0.39 mM). Specificity validation assays: Δ*T*2 (mSec) MR data displaying the lack of binding between (E) 2,6-SA-MRnS (10 μL, 7.5×10^{-3} M) and H5N1/HA1 (0–6×10^{-8} M) as well as between (F) 2,3-SA-MRnS (10 μL, 7.5×10^{-3} M) and H1N1/HA1 (0–10×10^{-9} M). These results demonstrate the influenza subtype targeting capability of our newly designed functional MRnS.

shown in Fig. 2B and D, respectively. The experimental K_d^* values for 2,6-SA- and 2,3-SA-MRnS were found to be 1.2 and 0.39 mM, respectively. The corresponding literature reports for K_d^* values both lie within the millimolar range,[11a] which directly reflects the success of using magnetic nanosensors for the assessment of binding interactions. In addition, computational analyses were performed using Autodock 4 to complement these assessments, and the observed K_d^* values were similar to those found experimentally, as shown in ESI Fig. S2–S6.† Taken together, these assays further confirmed our hypothesis regarding the rapid detection of influenza proteins using our functional MRnS. Next, to further demonstrate the specificity of this detection technique, our functional MRnS were cross-tested with the opposing HA variants (*e.g.*, 2,6-SA-MRnS were tested with H5N1/HA1 and 2,3-SA-MRnS were tested with H1N1/HA1). In order to accomplish this, PBS (1X, pH = 7.4) solutions (final volume of 500 μL) containing 2,6-SA-MRnS (10 μL, 7.5×10^{-3} M) was incubated for 15 minutes with increasing concentrations of H5N1/HA1 (0–6×10^{-8} M) (Fig. 2E). Similarly, solutions containing 2,3-SA-MRnS (10 μL, 7.5×10^{-3} M) were incubated for 15 minutes with increasing concentrations of H1N1/HA1 (0–1×10^{-8} M) (Fig. 2F). As expected, there was minimal to no binding in either scenario, verifying the ability of functional MRnS to differentiate between subtypes of influenza A.

2.3 Screening of entry blocker peptides

Once the binding between SA-conjugated MRnS and hemagglutinin had been analyzed, various entry blocker peptides (EBs) with reported binding affinities for both hemagglutinin variants (H1N1 and H5N1) were screened. EBs are currently a focus in the search for an effective anti-viral medication for influenza, as the virus has gained resistance to a number of anti-viral approaches, including disruption of genome transcription, and NA interference.[1,12,13] EBs would function as an anti-viral by preventing HA from binding to host cell receptors, thus preventing subsequent genomic entry. EBs selected for our experiments included EB Peptide, a broad-spectrum anti-viral shown to interact with HA1, and two additional sialic acid mimics, designated herein as ARLPR and Ste.[13c] The structures of these EBs can be found in ESI Fig. S2.† These EBs were functionalized with the surface carboxylic acid groups of IONPs using standard EDC/NHS chemistry,[14] as described in ESI Scheme S1.† The resulting EB Peptide- and ARLPR-conjugated MRnS (10 μL, 7.5×10^{-3} M) were first incubated at room temperature for 15 minutes in PBS solutions (1X, pH = 7.4, final volume of 500 μL) with increasing concentrations of H1N1/HA1 (0–10×10^{-8} M). As expected, each binding assay produced a positive trend of interaction, as shown in Fig. 3A and C. In addition, similar results were obtained when binding assays were conducted between H5N1/HA1 and EBs, and the results are shown in Fig. 3B and D. These results demonstrate the ability of selected EBs to bind with both variants of hemagglutinin. Subsequent competition assays were then conducted to determine experimental K_d^* values for EB Peptide and ARLPR. For H1N1/HA1 competition assays, PBS solutions (1X, pH = 7.4, final volume of 500 μL) were prepared containing constant concentrations of EB Peptide- or ARLPR-MRnS (10 μL, 7.5×10^{-3} M), H1N1/HA1 (1×10^{-8} and 3×10^{-8} M for EB Peptide and ARLPR solutions, respectively), and increasing concentrations of "free" EB Peptide (0–1.6×10^{-5} M) or "free" ARLPR (0–4.0×10^{-6} M), and incubated for 15 minutes at room temperature. Experimental K_d^* values for H1N1/HA1 binding with EB Peptide (Fig. 3E) and ARLPR (Fig. 3G) were 4.22 μM and 0.42 μM, respectively. It is worth noting that these values are very close to the reported literature values of 5–20 μM (ref. 13*a*) and 1.9 μM,[13c] respectively. For the H5N1 competition assays, similar PBS solutions were prepared containing constant concentrations of respective functional MRnS (10 μL, 7.5×10^{-3} M), H5N1/HA1 (3×10^{-8} M),

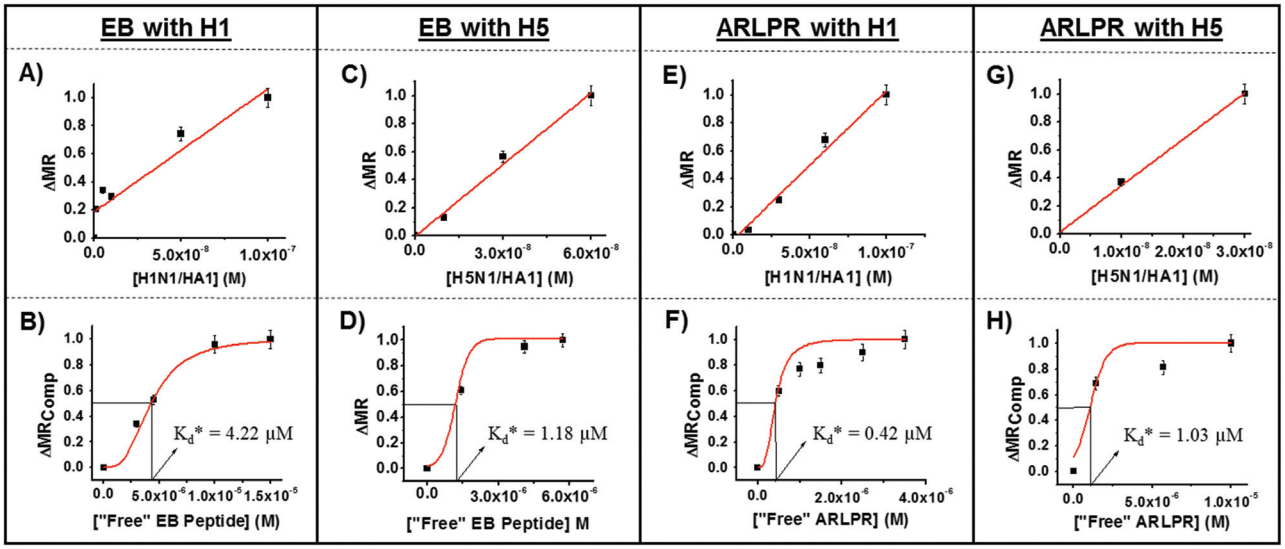

Fig. 3 Screening of EB peptides with binding affinity for HA. (A–D) Binding assay results between EB Peptide- and ARLPR-conjugated MRnS (10 μL, 7.5×10^{-3} M) with both hemagglutinin variants (concentrations ranging from 0–10×10^{-8} M), showing the expected linear binding trends. (E–H) Competition assays using MRnS (10 μL, 7.5×10^{-3} M), respective HA1 subunits (H1N1/HA1: 1×10^{-8} M and 3×10^{-8} M for EB Peptide and ARLPR solutions, respectively, and H5N1/HA1: 3×10^{-8} M for both) and "free" competitors (EB Peptide and ARLPR: micromolar concentration ranges), showing K_d^* values in the micromolar range. Compared to human lung cell receptor sialic acid, which possesses a K_d^* value in the millimolar range, these selected EB peptides exhibit higher binding affinities (1000 times stronger) for HA. These assays demonstrate the potential for these peptides to be used as therapeutic entry blocker agents. Furthermore, these MRnS-based bench-top assays may be used for further discovery of entry-blocker ligands.

and increasing concentrations of "free" EB Peptide (0–6.0×10^{-6} M) or "free" ARLPR (0–10.0×10^{-6} M), and were incubated for 15 minutes. The experimental K_d^* value for H5N1/HA1 binding with EB Peptide (Fig. 3F) was 1.18 μM and was compared to the literature values of 3–10 μM.[13a]

The literature value for ARLPR and H5N1/HA1 was not found, and so the experimental K_d^* value of 1.03 μM (Fig. 3H) was compared to the computational value obtained *via* Autodock 4, which was 52.05 μM. The remaining observed Autodock 4 findings are reported in ESI Fig. S3–S6.† These values allow for the comparison between entry blocker peptides, which is useful in the analysis of their capabilities as anti-viral drugs. Similar binding and competition assay results were obtained for Ste peptide and the results with H5N1/HA1 (K_d^* = 3.48 μM) are reported in ESI Fig. S7.† Taken together, these assays demonstrate the importance of using MR-based nanosensors for the development of new theranostic agents for the rapid containment of rising pathogenic strains of influenza.

2.4 Rapid detection of influenza

In order to determine how rapidly viral detection could be achieved using functional MRnS technology, time-dependent assays were conducted in which *T*2 MR values were collected throughout a period of 0–18 hours, with the earliest *T*2 MR data point being taken 5 minutes after mixing. EB Peptide and ARLPR were selected for this test due to their high binding affinity with HA. Two experimental solutions were prepared in PBS (1X, pH = 7.4, final volume of 500 μL), containing EB Peptide- and ARLPR-conjugated MRnS (10 μL, 7.5×10^{-3} M) and H1N1/HA1 (5×10^{-8} M). In addition, two control solutions were prepared in PBS (1X, pH = 7.4, final volume of 500 μL) containing only these functional MRnS (10 μL, 7.5×10^{-3} M). It is shown in Fig. 4 that although *T*2 values increased throughout the incubation period, a *T*2 change was detectable

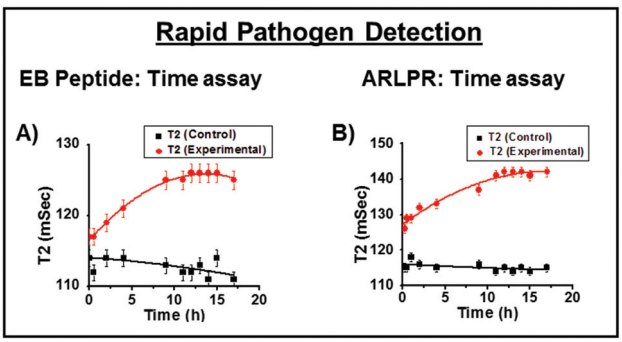

Fig. 4 Time-dependent assays were performed in order to demonstrate the rapid HA detection capability of our functional MRnS. (A) EB Peptide- and (B) ARLPR-conjugated MRnS (10 μL, 7.5×10^{-3} M) were used for detection of H1N1/HA1 (5×10^{-8} M), and the *T*2 MR data points were taken throughout an 18 h period starting with 5 minutes after mixing. The red lines represent the experimental solutions containing functional MRnS and H1N1/HA1, while the black lines represent the control solutions containing only functional MRnS. As shown in the figures, there were detectable *T*2 changes in both experimental solutions (red lines), immediately after mixing. This highlights the rapid detection capabilities of our MRnS technology.

immediately after mixing the functional MRnS and viral protein (H1N1/HA1). These results suggest that little to no incubation time is necessary for this rapid magnetic nanosensor-based diagnostic technique, highlighting its effectiveness in a clinical setting.

2.5 One-step differentiation between pathogenic and non-pathogenic influenza subtypes

Further considering the desired effectiveness of diagnostic techniques in clinical settings, it seemed apparent that the ability to conduct one diagnostic test capable of screening for multiple infections would be much more efficient than conducting many individual tests for each suspected infection. To accomplish this, a mixture of functional MRnS was created consisting of 2,6-SA- and 2,3-SA-conjugated IONPs with a ratio of 20/80, respectively. It was hypothesized that if a clinically influenza-infected sample (test solution) contained strictly H1N1/HA1, then only the 2,6-SA-MRnS would be able to interact with the target protein, producing a $\Delta T2$ MR equivalent to roughly 20% of the binding maximum (Fig. 5A). Alternatively, if the test solution was contaminated with strictly H5N1/HA1, it was expected that only 2,3-SA-MRnS would be able to bind to the target H5N1/HA1 protein, resulting in a $\Delta T2$ MR of roughly 80% maximum (Fig. 5B). Furthermore, if a clinical sample contained both hemagglutinin variants, it was anticipated that all of the functional MRnS (2,6- and 2,3-SA-MRnS) would interact with their respective viral protein, yielding a 100% binding interaction (Fig. 5C). To validate this hypothesis, three PBS solutions (1X, pH = 7.4, final volume of 500 μL) were prepared with the functional MRnS mixture (2,6- and 2,3-SA-MRnS, 10 μL, 7.5×10^{-3} M) and respective concentrations of H1N1/HA1 (3×10^{-8} M), H5N1/HA1 (3×10^{-8} M) or a combination of H1N1/HA1 and H5N1/HA1 (3×10^{-8} M each). $T2$ MR data were collected for each solution after a 15-minute incubation period, and the results are reported in Fig. 5D. As was expected, the test solutions containing only H1N1/HA1 and H5N1/HA1 resulted in roughly 20% (Fig. $5D_A$) and 65% (Fig. $5D_B$) binding, respectively, and 100% binding was obtained in the presence of both HA variants (Fig. $5D_C$). The fact that the theoretical 20/80% binding ratio was not perfectly

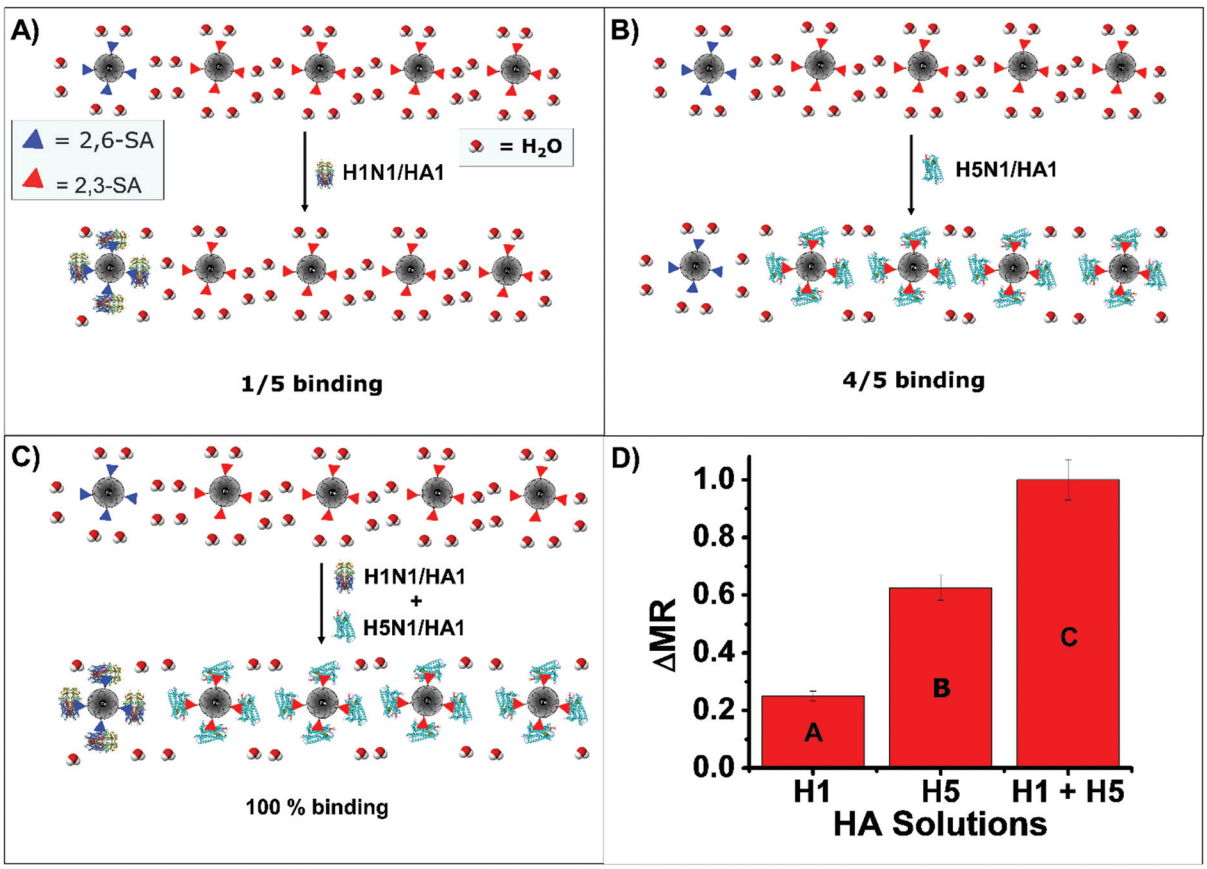

Fig. 5 Single-step detection of multiple influenza (HA) subtypes using a mixture of functional MRnS (20% 2,6-SA-MRnS and 80% 2,3-SA-MRnS). Schematic representations of (A) specific H1N1 detection *via* 20% binding within a sample infected with only H1N1/HA1 and (B) H5N1 detection *via* 80% binding within a sample infected with only H5N1/HA1. (C) Simultaneous detection of H1N1/HA1 and H5N1/HA1 in a co-infected sample *via* 100% binding. (D) Graphical representation of corresponding experimental results, obtained from solutions of MRnS mixture (10 μL, 7.5×10^{-3} M) and respective HA1 subunits (3×10^{-8} M), as expected. The fact that the ΔMR value for the H5N1/HA1 solution was slightly less than 0.8 (theoretical) can most likely be attributed to an uneven valency between the 2,6- and 2,3-conjugated IONPs. Nevertheless, it is evident that MRnS mixtures can be used to screen for multiple viral proteins, simultaneously.

achieved could be attributed to the different degree of 2,3-SA-conjugation with IONPs. The success of this experiment demonstrates the unique ability of our functional MRnS mixture to simultaneously screen for multiple pathogens. This diagnostic application of functional MRnS holds tremendous potential for expedited and high-throughput detection of infectious diseases in clinical settings.

3. Experimental section

3.1 Reagents

Ferric chloride hexahydrate, ferrous chloride tetrahydrate, hydrochloric acid and ammonium hydroxide were obtained from Fischer Scientific. DMF, DMSO, *N*-hydroxysuccinimide (NHS), carbonyl diimidazole (CDI), Polyacrylic acid (PAA) and other chemicals were purchased from Sigma-Aldrich. EDC (1-ethyl-3-[3-(dimethylamino) propyl] carbodiimide hydrochloride) was obtained from Pierce Biotechnology. The dialysis bag (MWCO 6–8 K) was purchased from Spectrum Labs. The 2,6- and 2,3-sialic acid were obtained from Carbosynth. EB Peptide, ARLPR, and Ste peptides were obtained from CreoSalus Advenced Tech. All Hemagglutinin HA1 subunits were obtained from Sino Biological Incorporated.

3.2 Instrumentations

Bruker's magnetic relaxometer mq20 (0.47 T) was used for *T*2 MR experiments. Malvern's Zetasizer-ZS90 was used for the size and zeta potential measurements of IONPs and functional MRnS. The magnetic column setup was purchased from Miltenyi Biotec.

3.3 Preparation of iron oxide nanoparticles (IONPs)

The IONPs were created by forming a core of iron salts, which was then surrounded by a coating of polyacrylic acid (PAA). Three solutions were first created in preparation for the synthesis. Solution 1 contained $FeCl_3$ (0.622 g), $FeCl_2$ (0.334 g) and H_2O (2 mL). Solution 2 contained NH_4OH (1.8 mL of 30% stock solution) and H_2O (15 mL). Solution 3 contained PAA (0.859 g) and H_2O (5 mL). Once the solutions were prepared, HCl (90 μL of 12 molar stock) was added to Solution 1, and then Solution 2 was immediately added to the mixture, while spinning. Then, Solution 3 was added and the resulting mixture was then vortexed for about an hour at 3000 RPM. After vortexing, the solution was centrifuged to get rid of bigger nanoparticles and agglomerates. The supernatant was collected, and dialysis was performed for purify the batch of IONPs, Scheme S1.†

3.4 Synthesis of α-2,6-sialic acid and α-2,3-sialic acid-conjugated IONPs (2,6-SA-MRnS and 2,3-SA-MRnS): CDI carbodiimide chemistry (Scheme S1†)

IONPs stock (5 mL) was diluted with PBS (5 mL). Two additive solutions were prepared prior to conjugation. Solution 1 contained carbonyldiimidazole (CDI, 0.5 mg) and DMSO (100 μL). Solution 2 contained α-2,6-sialic acid or α-2,3-sialic acid (10 μL of 10 μM stock), depending on desired product. Solution 1 was added dropwise to the IONP solution, followed by dropwise addition of Solution 2. The reaction mixture was placed on a tabletop mixer overnight. The final MRnS products were purified using magnetic column.

3.5 Synthesis of EB Peptide, ARLPR, and Ste-conjugated IONPs (EB-MRnS, ARLPR-MRnS and Ste-MRnS): water-soluble EDC/NHS carbodiimide chemistry

IONP stock (5 mL) was diluted with PBS (5 mL). Three additive solutions were prepared prior to conjugation. Solution 1 contained NHS (5 mg) and MES (250 μL). Solution 2 contained EB, ARLPR, or Ste (10 μL of 1 mM stock) depending upon desired product. Solution 3 contained EDC (8 mg) and MES (250 μL). Immediately after preparation of Solution 3, it was added in two portions to the IONP solution. Then, Solution 1 was added and incubated for 3 minutes with light mixing. Finally, Solution 2 was added in 10 μL segments, with light mixing. The resulting mixture was placed on a table-top mixer overnight. The final MRnS products were purified using magnetic column, Scheme S1.†

3.6 Procedure for MRnS binding assay

First, various solutions were prepared with varying concentrations of HA1 subunits (H1N1 or H5N1: ranging from 0–10×10^{-8} M). To each of these solutions was added a constant amount of MRnS (10 μL, 7.5×10^{-3} M). Solutions were allowed to incubate for 15–30 minutes before MRI analyses, although further MRI analyses was also utilized at time points ranging from 30 minutes to 24 h. A control solution was also created, which contained MRnS but no HA1. These experiments were carried out to measure control *T*2 values which were then used as baselines.

3.7 Procedure for "free" ligand competition assay

Various solutions were prepared, each containing equivalent concentration of HA1 (0–6×10^{-8} M) and MRnS (10 μL, 7.5×10^{-3} M). To these solutions, increasing amounts of "free" competitor was added (0–3×10^{-3} M and 0–15×10^{-6} M for sialic acid ligands and EBs, respectively) in order to disrupt binding between the MRnS and HA1. Desired concentrations of "free" competitor varied depending on the competitor in use, and chosen concentrations generally fell within a range of the literature K_d values for the competitor-HA1 binding. Two control solutions were created. Control 1 contained only MRnS. Control 2 contained MRnS, HA1, but no "free" competitor. These controls were designed to emulate full binding, and a state of zero binding.

3.8 Magnetic relaxation (MR) experiments

The measurement of spin–spin relaxation times, designated as "*T*2," was done using a 0.47T mq20 NMR analyzer (Minispec, Bruker, Germany). *T*2 data was collected in triplicate for each sample, and the average was used for data plotting. An example of raw *T*2 data is shown in ESI Fig. S8.†

3.9 Data analysis

Plots were created using Origin. Binding assay plots were equipped with a trend line using linear fitting, and competition assays were equipped with a sigmoidal curve using a Boltzmann "best-fit" algorithm. $\Delta T2$ MR data is obtained based upon the use of the baseline $T2$ value (mSec), obtained from solutions having no HA1 subunit. The $T2$ baseline value is not converted into the resulting ΔMR-normalized graph, and so each graphical point represents a solution containing HA1 (either H1 or H5). For binding assay normalization, ΔMR representation is achieved by dividing the $\Delta T2$ value of samples with varying amounts of HA ($\Delta T2_{HA}$) by the $\Delta T2$ value associated with the most concentrated HA solution ($\Delta T2_{Max}$). The full equation appears as such: $\Delta MR = \frac{\Delta T2_{HA}}{\Delta T2_{Max}}$. After normalization, the graph shows a linear increase in ΔMR values under ideal binding conditions. For competition assay data, ΔMR_{Comp} normalization is achieved by subtracting the $\Delta T2$ values recorded with various concentrations of "free" competitor ($\Delta T2_{Comp}$) from the $\Delta T2$ value associated with the solution having no "free" competitor ($\Delta T2^0_{Max}$), thus scaling the range of values down to zero. This data is then divided by the $\Delta T2^0_{Max}$, providing a range of ΔMR_{Comp} values between 0 and 1. The full equation appears as such: $\Delta MR_{Comp} = \frac{\Delta T2^0_{Max} - \Delta T2_{Comp}}{\Delta T2^0_{Max}}$. The ligand concentration at which the ΔMR_{Comp} value is equal to 0.5 represents the K^*_d value.

4. Conclusions

In summary, we have designed novel magnetic nanosensors capable of detecting influenza-associated proteins with detection thresholds as little as 1.0 nM within minutes, while maintaining the degree of specificity required to distinguish between influenza subtypes. These results demonstrate that MRnS diagnostic tools have higher specificity and sensitivity, as well as lower turnaround times than the current diagnostic methods, including RT-PCR, ELISA and viral culturing. We have also shown that our functional MRnS provide an alternative method for the analysis of binding interactions, which is highly important in the search for effective therapeutics, including entry blocker peptides. Using this technique, we were able to experimentally determine apparent K^*_d values for binding interactions between HA proteins and sialic acid cell receptors as well as entry blocker peptides, including EB Peptide, ARLPL, and Ste. Our MRnS-based experimentally derived K^*_d values for the cell receptors and EBs were in the milli- and micromolar range, respectively, which is in accordance with both the literature reported values, and those observed *via* Autodock 4. Additionally, it has been shown that MRnS can be used in mixtures to screen for multiple pathogens at once. This novel technique would discard the need to conduct many individual tests, saving time and resources. The success of this technique was demonstrated by the ability of our 20/80 mixture of 2,6-SA- and 2,3-SA-conjugated MRnS to easily distinguish between subtypes of influenza (H1N1 and H5N1), as well as to detect both HA variants when used in a co-infected sample. This innovative application of MRnS technology provides an effective and high-throughput method for the simultaneous detection and diagnosis of a wide spectrum of infectious diseases in clinical settings. Together, MRnS's sensitivity, specificity, point-of-care simplicity, low cost, and ease of deployment make a strong case for the implementation of diagnostic nanosensors in both clinical and laboratory settings.

Acknowledgements

This work is also supported by K-INBRE P20GM103418, ACS PRF 56629-UNI7 and PSU polymer chemistry Start Up fund, all to SS. We thank Mr Roger Heckert and Mrs Katha Heckert for their generous donations towards our laboratory research. We thank the Chair of the Chemistry Department, Dr Petar Dvornic, and Professor of Chemistry, Dr James McAfee, for insightful discussions and state-of-the-art research infrastructures.

Notes and references

1 J. Yang, M. Li, X. Shen and S. Liu, *Viruses*, 2013, **5**, 352.
2 S. Kumar and K. J. Henrickson, *Clin. Microbiol. Rev.*, 2012, **25**, 344.
3 (*a*) T. F. Hatchette, S. J. Drews, N. Bastien, Y. Li, G. German, N. Antonishyn, H. Charest, T. Mazzulli, K. Fonseca, M. Krajden, M. Petric, K. Dust and J. J. LeBlanc, *J. Clin. Microbiol.*, 2013, **51**, 3835; (*b*) J. B. Mahony, *Clin. Microbiol. Rev.*, 2008, **21**, 716; (*c*) W. Chen, B. He, C. Li, X. Zhang, W. Wu, X. Yin, B. Fan, X. Fan and J. Wang, *J. Med. Microbiol.*, 2007, **56**, 603.
4 M. L. Sin, K. E. Mach, P. K. Wong and J. C. Liao, *Expert Rev. Mol. Diagn.*, 2014, **14**, 225.
5 C. Kaittanis, H. Boukhriss, S. Santra, S. A. Naser and J. M. Perez, *PLoS One*, 2012, **7**, e35326.
6 M. Liong, A. N. Hoang, J. Chung, N. Gural, C. B. Ford, C. Min, R. R. Shah, R. Ahmad, M. Fernandez-Suarez, S. M. Fortune, M. Toner, H. Lee and R. Weissleder, *Nat. Commun.*, 2013, **4**, 1752.
7 W. W. Ye, M. K. Tsang, X. Liu, M. Yang and J. Hao, *Small*, 2014, **10**, 2390.
8 J. M. Perez, F. J. Simeone, Y. Saeki, L. Josephson and R. Weissleder, *J. Am. Chem. Soc.*, 2003, **125**, 10192.
9 (*a*) K. El-Boubbou, C. Gruden and X. Huang, *J. Am. Chem. Soc.*, 2007, **129**, 13392; (*b*) C. Kaittanis, S. A. Naser and J. M. Perez, *Nano Lett.*, 2007, **7**, 380; (*c*) L. S. Lin, Z. X. Cong, J. B. Cao, K. M. Ke, Q. L. Peng, J. Gao, H. H. Yang, G. Liu and X. Chen, *ACS Nano*, 2014, **8**, 3876; (*d*) C. Kaittanis, S. Santra and J. M. Perez, *J. Am. Chem. Soc.*, 2009, **131**, 12780; (*e*) J. Liu, Y. Liu, W. Bu, J. Bu, Y. Sun, J. Du and

J. Shi, *J. Am. Chem. Soc.*, 2014, **136**, 9701; (*f*) J. B. Haun, N. K. Devaraj, B. S. Marinelli, H. Lee and R. Weissleder, *ACS Nano*, 2011, **5**, 3204; (*g*) O. J. Santiesteban, C. Kaittanis and J. M. Perez, *Small*, 2014, **10**, 1202; (*h*) O. J. Santiesteban, C. Kaittanis and J. M. Perez, *Angew. Chem., Int. Ed.*, 2012, **51**, 6728; (*i*) Y. Chen, Y. Xianyu, Y. Wang, X. Zhang, R. Cha, J. Sun and X. Jiang, *ACS Nano*, 2015, **9**, 3184; (*j*) X. Zhao, R. Tapec-Dytioco and W. Tan, *J. Am. Chem. Soc.*, 2003, **125**, 11474; (*k*) X. Xue, F. Wang and X. Liu, *J. Am. Chem. Soc.*, 2008, **130**, 3244; (*l*) X. Liu, Z. Wu, Q. Zhang, W. Zhao, C. Zong and H. Gai, *Anal. Chem.*, 2016, **88**, 2119.

10 W. Wu and G. M. Air, *Virology*, 2004, **325**, 340.

11 (*a*) C. Sieben, C. Kappel, R. Zhu, A. Wozniak, C. Rankl, P. Hinterdorfer, H. Grubmuller and A. Herrmann, *Proc. Natl. Acad. Sci. U. S. A.*, 2012, **109**, 13626; (*b*) N. K. Sauter, M. D. Bednarski, B. A. Wurzburg, J. E. Hanson, G. M. Whitesides, J. J. Skehel and D. C. Wiley, *Biochemistry*, 1989, **28**, 8388; (*c*) C. McCullough, M. Wang, L. Rong and M. Caffrey, *PLoS One*, 2012, **7**, e33958.

12 T. Matsubara, A. Onishi, T. Saito, A. Shimada, H. Inoue, T. Taki, K. Nagata, Y. Okahata and T. Sato, *J. Med. Chem.*, 2010, **53**, 4441.

13 (*a*) J. C. Jones, E. A. Turpin, H. Bultmann, C. R. Brandt and S. Schultz-Cherry, *J. Virol.*, 2006, **80**, 11960; (*b*) Q. Liu, D. Y. Liu and Z. Q. Yang, *Acta Pharmacol. Sin.*, 2013, **34**, 1257; (*c*) X. Shen, X. Zhang and S. Liu, *J. Thorac. Dis.*, 2013, **5**, S149.

14 C. Kaittanis, S. Santra, O. J. Santiesteban, T. J. Henderson and J. M. Perez, *J. Am. Chem. Soc.*, 2011, **133**, 3668.